IEEE Access
Multidisciplinary | Rapid Review | Open Access Journal

Received November 29, 2018, accepted December 13, 2018, date of publication January 16, 2019, date of current version January 29, 2019.

Digital Object Identifier 10.1109/ACCESS.2018.2889345

Voltage Balancing Control of IPOS Modular Dual Active Bridge DC/DC Converters Based on Hierarchical Sliding Mode Control

SANGMIN LEE[1], YOON-CHEUL JEUNG[2], (Student Member, IEEE), AND DONG-CHOON LEE[2], (Senior Member, IEEE)

[1]Doosan Robotics Inc., Suwon 16648, South Korea
[2]Department of Electrical Engineering, Yeungnam University, Gyeongsan 38541, South Korea

Corresponding author: Dong-Choon Lee (dclee@yu.ac.kr)

This work was supported by the Yeungnam University Research Grant in 2016.

ABSTRACT This paper proposes a novel nonlinear control method for the input-parallel output-series modular dual active bridge (DAB) dc/dc converter which regulates the dc-bus voltage and individual module voltages together. At first, a state space form of the DAB converter model is derived. Next, the output voltage controller of the modular DAB converter is designed with the hierarchical sliding-mode control theory. Furthermore, due to the robustness of the sliding-mode control, the control performance is insensitive to the mismatch of leakage inductances of the DAB transformers. The feasibility of the proposed control scheme has been proved by simulation and experimental results.

INDEX TERMS Dual active bridge, modular dc/dc converter, hierarchical sliding mode control, voltage balancing control.

I. INTRODUCTION

Recently, a great attention has been paid to the high power isolated DC/DC converters used for industry applications such as DC transmission and distribution power systems, solid-state transformers, and energy storage systems (ESS) [1]–[4]. For the requirements of the system, the power capacity of the modular converter can be expanded by series or parallel connections of the input and output terminals. Also, the reliability of the modular converter system can be improved by using redundant modules.

The dual active bridge (DAB) circuit is a type of isolated DC/DC converters which has the soft switching features and bi-directional power flows [5]–[7]. Due to these advantages, the DAB converter can be adopted as a basic unit for modular structure of converters [3], [8]–[10]. In this work, the input-parallel output-serial (IPOS) modular DAB converter is investigated, rather than a single DAB unit. The role of the IPOS modular DAB converter is to regulate the power flow between the low-voltage DC (LVDC) bus and the medium-voltage DC (MVDC) bus [11], [12].

In the case of the output-series connection, the output voltages of individual modules are often unbalanced due to the parameter mismatches in transformer turn ratios, leakage inductances, internal resistances and so on, even though the overall DC-bus voltage is well controlled [3], [8]–[10]. Thus, it is needed to control the output voltages of the individual modules to be balanced.

For this purpose, in the modular structure of DC-DC converters, the droop-based output voltage control has been proposed [13], [14], where the DC-bus voltage controller is applied to regulate the MVDC voltage and the voltage references of the individual modules are adjusted by the droop gains depending on the output current. Although this method is simple to implement, an additional current sensor is required for each module. In [15]–[18], the output voltages of the individual modules are controlled through the master-slave controller, where the output voltage references of the slave modules are generated from the controller of the master module. At the same time, a slave controller is needed for each slave module, which controls its output voltage to be equal to that of the master module. As a result, the output voltages of individual modules can be balanced. However, this method requires a very high reliability of the master controller. Since each module in the modular converter is controlled by the slave controller of individual modules (where the reference signal of the slave controller is generated

from the master controller,) based on the master controller, the whole converter system does not work if the master controller fails. On the other hand, the model predictive control (MPC) [19] was suggested for the voltage balancing of individual modules, which adopts the PI controllers for the DC-bus voltage control. In this scheme, the control performance of the converter is affected by the parameter perturbation of the model.

Meanwhile, the advanced control schemes such as MPC [20], feedback linearization [21], fuzzy logic [22], observer-based nonlinear control [23], and sliding mode control (SMC) [24], [25] have been proposed to enhance the control performance of the DAB converter. However, the target system of these control methods is not a modular type but a single DAB circuit.

For the IPOS modular DAB converter, both the DC-bus voltage controller and the module voltage or current controllers are often required for the balanced load power sharing between individual modules [26], [27]. In general, a cascaded structure of two closed-loop PI controllers is used to balance the output power of individual modules [3], [8], [9]. However, the conventional linear controllers cannot guarantee the control performance for various operating conditions since the DAB converter has a nonlinear characteristic. In addition, system dynamics become slow due to the low bandwidth of the outer control loop. To avoid this problem, a master-slave control scheme has been proposed in [10]. However, this kind of control scheme has the reliability issue as aforementioned. So, it is necessary to develop a new control method not only which is robust to parameter disturbances with fast responses, but also which can provide a balanced power sharing and output voltage regulation capability.

As far as authors know, the DC-bus voltage control scheme with a module voltage balancing control based on the HSMC for the IPOS modular DAB converter has never been studied except [28], from which this manuscript has been expanded with more analysis and test results.

In this paper, a novel nonlinear voltage controller is proposed for the IPOS modular DAB DC/DC converter. First, the nonlinear model of the converter is derived in a state-space form, where the single phase-shift modulation (SPSM) is applied. Next, a nonlinear controller for the DC-bust voltage as well as individual module voltages is designed, based on the hierarchical sliding mode control (HSMC) theory. In addition, the effects of the mismatch of leakage inductances of two DAB modules on the control performance is investigated. Finally, the validity of the proposed control method is verified by simulation and experimental results.

II. IPOS MODULAR DAB CONVERTERS

A. DESCRIPTION OF IPOS MODULAR DAB CONVERTERS

The input terminals of the DAB modules are connected in parallel on the LVDC bus side and the output terminals are connected in series on the MVDC bus side, which is shown in Fig. 1. Fig. 2 shows the IPOS modular DAB converter,

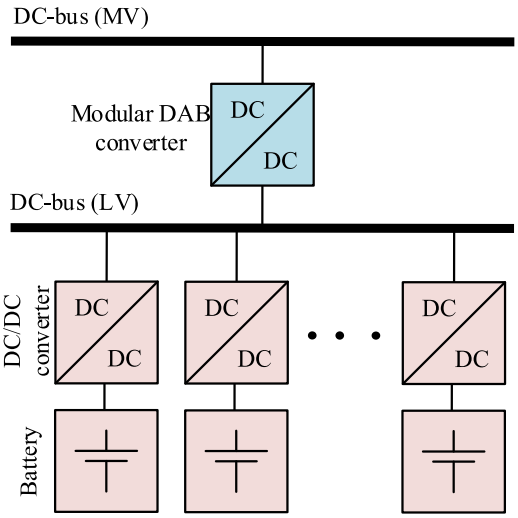

FIGURE 1. A two-stage DC/DC conversion system.

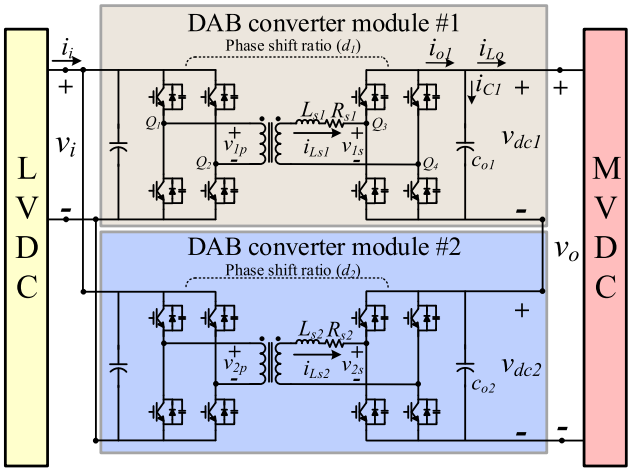

FIGURE 2. IPOS modular DAB DC/DC converter.

where the number of modules is two. Each DAB module consists of one high-frequency transformer and four IGBT legs. In Fig. 2, the meanings of symbols are as follows:

- v_i and v_o are the input and output voltages of the modular IPOS DAB converter,
- v_{1p} and v_{2p} are the primary voltages of transformers,
- v_{1s}, and v_{2s} are the secondary voltages of transformers,
- v_{dc1} and v_{dc2} are the output voltages of DAB modules,
- i_{Ls1} and i_{Ls2} are the inductor currents of transformers,
- L_{s1} and L_{s2} are the equivalent leakage inductances of transformers,
- R_{s1} and R_{s2} are the internal resistances of transformers and inductors,
- C_{o1} and C_{o2} are the output capacitances of DAB modules,
- d_1 and d_2 are the phase-shift ratios for DAB modules.

The single DAB module in the IPOS modular converter can be regarded as a single-input multi-output (SIMO) system since the phase-shift ratio is set as an input and both the

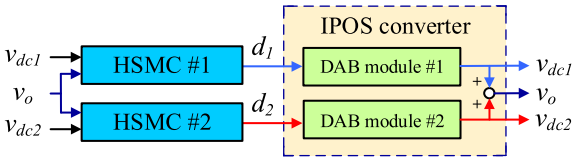

FIGURE 3. Proposed control structure of IPOS modular DAB converter.

DAB module voltage and the overall DC-bus voltage can be selected as outputs.

Fig. 3 shows a configuration of the proposed control structure of the IPOS modular DAB converter, which is based on the HSMC. The input variables of the IPOS converter model are duty ratios of two modules and its output variables are each module voltage and the DC-bus voltage. The duty ratios are decided from the control laws, which will be derived in the later section.

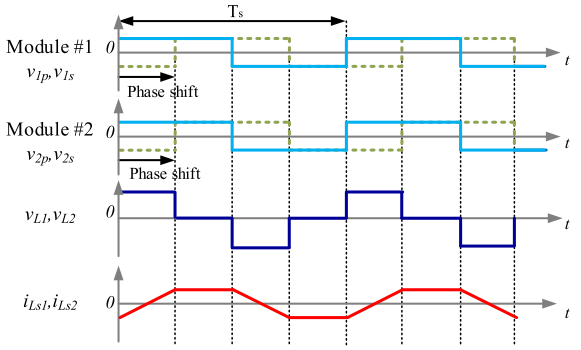

FIGURE 4. Single phase-shift modulation for IPOS modular converter.

B. SINGLE PHASE-SHIFT MODULATION OF IPOS DAB CONVERTERS

In this research, the single phase-shift modulation(SPSM) is used to control the IPOS modular DAB converter. Fig. 4 shows the operating waveforms of the SPSM, where it is assumed that the carrier waveforms for two DAB modules are identical with no phase shift each other for a simple modeling and that the transformer turn ratio is one to one. The output power is controlled by the phase-shift ratio between v_{1p} and v_{1s}. In the operation of the SPSM, all the switches of the DAB converter are operated at a fixed duty ratio of 0.5, and the upper and lower switches in one leg are operated complementarily. The average output power of the single DAB module #1, P_{o1}, is given by [29], [30]

$$P_{o1} = N_1 \frac{v_{1p} v_{1s}}{2 f_s L_{s1}} d_1 (1 - d_1), \tag{1}$$

where, N_1 is the transformer turn ratio (approximately equal to v_{1s}/v_{1p}) and f_s $(=1/T_s)$ is the switching frequency. The total output power of the IPOS modular converter, as shown in Fig. 2, is double that of the single DAB module.

C. MODELING OF IPOS MODULAR DAB CONVERTERS

The normalized state-space model for the output voltage of the conventional DAB converter based on the SPSM has been derived in [31], where the fundamental component ($k=0$) only is considered for simplicity since the sliding mode control is insensitive to the model uncertainty of the system [32], [33]. According to [31], there is only 3% error in average output powers between the approximated fundamental-component-based-model analysis and the circuit-model simulation. Also, this approximation of harmonic modeling for the single DAB converter has been applied successfully in [12].

The mathematical model for the output voltage of DAB module #1 is obtained as

$$\frac{dv_{dc1}(t)}{dt} = -\frac{8}{C_{o1}\pi^2} \frac{\cos\{\varphi_z(0)\}}{|z(0)|} v_{dc1}(t) + \frac{8}{C_{o1}\pi^2} \frac{N_1 v_i(t)}{|z(0)|} \cos\{\delta_1 - \varphi_z(0)\} - \frac{i_{Lo}(t)}{C_{o1}}, \tag{2}$$

where the impedance $|z(0)|$ and the impedance angle $\varphi_z(0)$ on the secondary side of the transformer are expressed, respectively, as

$$|z(0)| = \sqrt{R_{s1}^2 + (\omega_s L_{s1})^2} \tag{3}$$

$$\varphi_z(0) = \tan^{-1}\left(\frac{\omega_s L_{s1}}{R_{s1}}\right), \tag{4}$$

where "0" represents the fundamental component of the switching frequency.

Expressing (2) in a state-space form,

$$\dot{x}_1 = f_1(x_1) + g_1(x_1) u_1 + E_1, \tag{5}$$

where x_1 is the output voltage of module #1 and

$$f_1(x_1) = -\frac{8}{C_{o1}\pi^2} \frac{\cos\{\varphi_z(0)\}}{|z(0)|} v_{dc1}(t), \tag{6}$$

$$g_1(x_1) = \frac{8}{C_{o1}\pi^2} \frac{N_1}{|z(0)|} v_i(t), \tag{7}$$

$$E_1 = -\frac{i_{Lo}(t)}{C_{o1}}. \tag{8}$$

The input variable of module #1 can be selected as [12],

$$u_1 = \cos\{\delta_1 - \varphi_z(0) + \delta_{in}\}. \tag{9}$$

where δ_1 is the phase shift angle and δ_{in} is its initial value. If δ_{in} is selected as

$$\delta_{in} = -\pi/2 + \varphi_z(0), \tag{10}$$

then, the input u_1 is obtained as

$$u_1 = \sin(\delta_1). \tag{11}$$

The mathematical model of module #2 can be derived in the same procedure as above.

Next, the mathematical model of the IPOS modular converter is derived as follows. Assuming that the parameters of

the two modules are the same, from (2), the output voltage of the IPOS modular converter can be expressed as

$$\frac{dv_o(t)}{dt} = -\frac{8}{C_{o1}\pi^2}\frac{\cos\{\varphi_z(0)\}}{|z(0)|}v_o(t) + \frac{8}{C_{o1}\pi^2}\frac{N_1 v_i(t)}{|z(0)|}\sin(\delta_o) - 2\frac{i_{Lo}(t)}{C_{o1}}. \quad (12)$$

If (12) is expressed in a state-space form, we can obtain

$$\dot{x}_o = f_o(x_o) + g_o(x_o)u_o + E_o, \quad (13)$$

where x_o is the DC-bus voltage and

$$f_o(x_o) = -\frac{8}{C_{o1}\pi^2}\frac{\cos\{\varphi_z(0)\}}{|z(0)|}v_o(t), \quad (14)$$

$$g_o(x_o) = \frac{8}{C_{o1}\pi^2}\frac{N_1}{|z(0)|}v_i(t), \quad (15)$$

$$E_o = -2\frac{i_{Lo}(t)}{C_{o1}}, \quad (16)$$

$$u_o = \sin(\delta_o). \quad (17)$$

III. PROPOSED HIERARCHICAL SLIDING MODE CONTROLLER

The sliding mode control allows the system to reach the predetermined sliding surface irrespective of the initial conditions given in the system [34]. There are three steps in the controller design using the SMC. At first, the state variable is controlled so as to reach the specified surface regardless of its initial condition, thereafter to stay on the sliding surface. Eventually, the state variable is controlled so as to converge to the equilibrium point along the sliding surface.

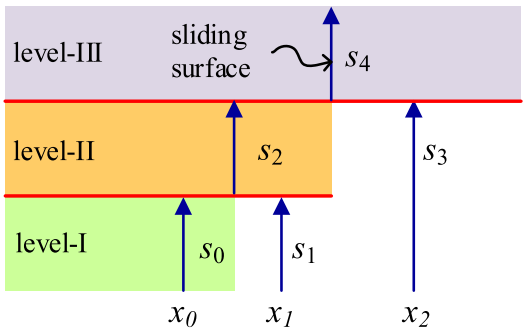

FIGURE 5. Structure of hierarchical sliding surfaces.

In the HSMC scheme, sliding surfaces can be designed in a hierarchical structure [35], [36]. Fig. 5 shows an example of the hierarchical sliding surfaces, where x_0, x_1, and x_2 are the state variables and s_0, s_1, s_2, s_3, and s_4 are the sliding surfaces. Now, let's consider the SIMO system with one input and two state variables, x_0 and x_1. The mathematical models corresponding to x_0 and x_1 can be regarded as subsystems. The sliding surfaces of s_0 and s_1 in level-I can be designed with state variables of x_0 and x_1 based on the SMC theory. Then, the two sliding surfaces of s_0 and s_1 can be combined to make a new sliding surface s_2 in level-II, which generates a control law for the SIMO system. If another state variable x_2 is involved, a new sliding surface s_4 in level-III can also be made.

A. DESIGN OF HSMC

In this subsection, the hierarchical sliding mode controller of level-II for the IPOS converter is designed to regulate the output voltages as well as balance the output voltages of DAB modules.

Firstly, two sliding surfaces of level-I for module #1 are selected as

$$s_o = c_1 e_o + c_2 \int e_o dt, \quad (18)$$

and

$$s_1 = c_3 e_1 + c_4 \int e_1 dt, \quad (19)$$

where s_o and s_1 represent the sliding surfaces of the DC-bus voltage (v_o) and the module output voltage (v_{dc1}) of module #1, respectively, e_0 and e_1 are the regulation errors, and $c_1 - c_4$ are the controller gains.

Taking a derivative of (18) and (19) to obtain the equivalent control input of the SMC, then

$$\dot{s}_o = c_1\dot{e}_o + c_2 e_o, \quad (20)$$

and

$$\dot{s}_1 = c_3\dot{e}_1 + c_4 e_1, \quad (21)$$

where $\dot{s}$ and $\dot{e}$ represent the derivative of the sliding surface and regulation error, respectively.

From (5) and (13), the derivative of the regulation error can be expressed as

$$\dot{e}_o = \dot{x}_o - \dot{x}_{od} = f_o(x_o) + g_o(x_o)u_o + E_o, \quad (22)$$

and

$$\dot{e}_1 = \dot{x}_1 - \dot{x}_{1d} = f_1(x_1) + g_1(x_1)u_1 + E_1, \quad (23)$$

where x_{od} and x_{1d} are the references of the DC-bus voltage and the module output voltage, of which derivatives are assumed to be zero ($\dot{x}_{od} = \dot{x}_{1d} = 0$).

Secondly, the equivalent control inputs that determine the dynamics of the system on the sliding surface are derived. Substituting (22) into (20),

$$\dot{s}_o = c_1\{f_o(x_o) + g_o(x_o)u_o + E_o\} + c_2 e_o. \quad (24)$$

In (24), the equivalent control input (u_o) can be obtained by setting the derivative of the sliding surface as zero, which is obtained as

$$u_o = \frac{-c_1 f_o(x_o) - c_1 E_o - c_2 e_o}{c_1 g_o(x_o)}. \quad (25)$$

In the same way, another control input, u_1, is obtained as

$$u_1 = \frac{-c_3 f_1(x_1) - c_3 E_1 - c_4 e_1}{c_3 g_1(x_1)}. \quad (26)$$

Next, the equivalent control inputs of level-II are derived as follows. The sliding surface of level-II, s_2, is selected by a linear combination of the sliding surfaces of level-I as [35]

$$s_2 = s_o + \alpha s_1, \tag{27}$$

where α is the control gain.

To make the states of the system reach the sliding surface and to ensure the asymptotic stability, the equivalent control input (u_{eq1}) for level-II for module #1, which is composed of equivalent control laws of level-I and a switching control input, can be selected as [35]

$$u_{eq1} = u_o + u_1 + u_{sw}. \tag{28}$$

In order to derive the u_{sw}, from (22), (23), (27) and (28), the derivative of sliding surface of level-II can be manipulated as

$$\begin{aligned}\dot{s}_2 &= c_1\dot{e}_o + c_2 e_o + \alpha(c_3\dot{e}_1 + c_4 e_1)\\ &= c_1\{f_o(x_o) + g_o(x_o)u_{eq} + E_o\} + c_2 e_o\\ &\quad + \alpha[c_3\{f_1(x_1) + g_1(x_1)u_{eq} + E_1\} + c_4 e_1]\\ &= c_1\{f_o(x_o) + g_o(x_o)(u_o + u_1 + u_{sw}) + E_o\}\\ &\quad + c_2 e_o + \alpha[c_3\{f_1(x_1) + g_1(x_1)(u_o + u_1 + u_{sw}) + E_1\} + c_4 e_1]\\ &= c_1 g_o(x_o)u_o + c_1 g_o(x_o)u_{sw} + \alpha[c_3 g_1(x_1)u_1 + c_3 g_1(x_1)u_{sw}],\end{aligned} \tag{29}$$

where the control inputs, u_0 and u_1, in (22) and (23), respectively, need to be replaced by the u_{eq} since there is only a single input for the SIMO system.

The reaching law (ξ), which characterizes how the state variable approaches to the sliding surface of level-II, can be chosen with the signum function (sgn), as [35]

$$\xi = -ms_2 - n \cdot sgn(s_2), \tag{30}$$

where m and n are the HSMC gains, and the sgn function is defined as follows:

$$sgn(s_2) = \begin{cases} 1 & (s_2 > 0) \\ 0 & (s_2 = 0) \\ -1 & (s_2 < 0). \end{cases} \tag{31}$$

To avoid the chattering phenomenon, the "sgn" function is usually replaced by a hyperbolic function ($tanh$) as [12]

$$sgn(s_2) = tanh(s_2) \tag{32}$$

Setting (29) equal to (30) and applying the relation of (32),

$$\begin{aligned}c_1 g_o(x_o)u_o + \alpha c_3 g_1(x_1)u_1 + [c_1 g_o(x_o) + \alpha c_3 g_1(x_1)]u_{sw}\\ = -ntanh(s_2) - ms_2\end{aligned} \tag{33}$$

Then, the switching control input of level-II is obtained as

$$u_{sw} = \frac{-c_1 g_o(x_o)u_1 - \alpha c_3 g_1(x_1)u_o - n\tanh(s_2) - ms_2}{c_1 g_o(x_o) + \alpha c_3 g_1(x_1)} \tag{34}$$

Substituting (25), (26) and (34) into (28), the resultant control input for level-II is derived as

$$u^*_{eq1} = \frac{1}{c_1 g_o(x_o) + \alpha c_3 g_1(x_1)} \begin{bmatrix} -(c_1 f_o(x_o) + c_1 E_o + c_2 e_o) \\ -\alpha(c_3 f_1(x_1) + c_3 E_1 + c_4 e_1) \\ -(ntanh(s_2) + ms_2) \end{bmatrix} \tag{35}$$

From (11), (17) and (35), the phase shift ratio of the DAB converter #1 is calculated as

$$d_1^* = \frac{\delta_0^*}{\pi} = \frac{\sin^{-1}(u^*_{eq1})}{\pi} \tag{36}$$

where the range of the phase shift ratio is from -0.5 to 0.5.

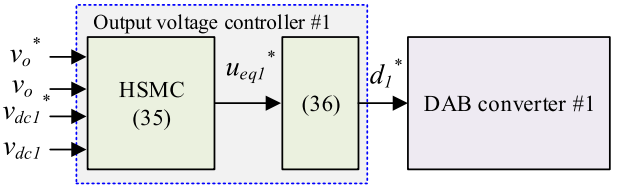

FIGURE 6. Representation of the proposed control scheme for DAB converter.

From the above, the simplified block diagram of the proposed control scheme for DAB module #1 can be drawn as in Fig. 6. The voltage controller of module #2 also can be applied as above.

B. EXISTENCE CONDITION OF HSMC

The existence condition of the HSMC can be verified by the Lyapunov's criteria. From (27) and (30), then,

$$\dot{V} = s_2\dot{s}_2 = (s_o + \alpha s_1)(-n\text{sgn}(s_2) - ms_2). \tag{37}$$

If the gains of n, m and α are all positive, the Lyapunov function is always negative. So, the existence condition of the HSMC is satisfied, which means that the control loop is asymptotically stable.

TABLE 1. Parameters of IPOS modular DAB converter (simulation).

Parameters	Values
Rated power	1 MW
LVDC bus voltage	1000 V
MVDC bus voltage	2000V
Number of modules	2

IV. SIMULATION RESULTS

To prove the validness of the proposed controller, simulations have been performed using PSIM software. The system parameters for simulations are listed in Table 1 and 2. The IPOS modular DAB converter circuit consists of two DAB modules with different leakage inductance values, which are 50μH and 60μH, respectively.

TABLE 2. Parameters of single DAB module (simulation).

Parameters	Values
Rated power	500 kW
Input DC voltage (v_i)	1000 V
Output DC voltage (v_{dc1}, v_{dc2})	1000 V
Transformer turn ratio	1 : 1
Equivalent series inductance of transformer referred to secondary side (L_{s1}, L_{s2})	50μH, 60μH
Output capacitance	1000 μF

Since there is no explicit rule to determine the SMC controller gains [34], the HSM controller gains ($c_1 = c_3 = 0.0000324$, $c_2 = c_4 = 0.01275$, $n = 1$, $m = 6750$) were obtained by a trial and error, which satisfy the existence condition of sliding surfaces. For performance comparison, the PI controller is employed, where the PI gains ($\omega_c = 450Hz$) are selected by small signal analysis [31], which are given as follows:

- Gains of DC-bus voltage controller: $k_{p,bus} = 1.567 \times 10^{-3}$, $k_{i,bus} = 0.3969$
- Gains of balancing controller: $k_p = 3.13 \times 10^{-3}$, $k_i = 1.5768$

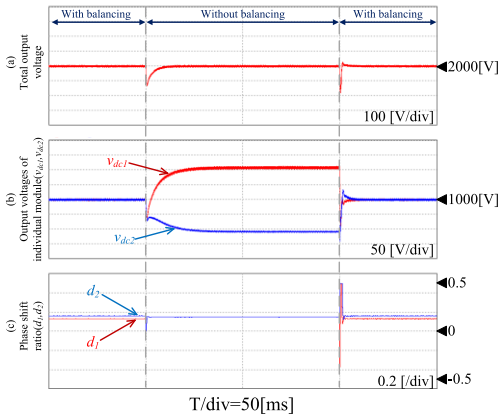

FIGURE 7. Control performances of with and without balancing control under unequal inductance (Ls2 > Ls1). (a) DC-bus voltage. (b) Output voltages of two modules. (c) Phase-shift ratios of two modules.

Fig. 7 shows the control performance in the cases of with and without the balancing control under different inductance conditions ($L_{s2} > L_{s1}$). Fig. 7(a) and (b) show the DC-bus voltage and the two module voltages, respectively. The DC-bus voltage is well controlled regardless of the balancing control of each DAB module. However, the output voltages of the DAB modules are unequal when the balancing control is not applied. Fig. 7(c) shows the phase-shift ratios of the two DAB modules, where d_1 and d_2 become different each other since the leakage inductances are set differently. However, when the balancing control is not applied, the d_1 and d_2 are exactly the same.

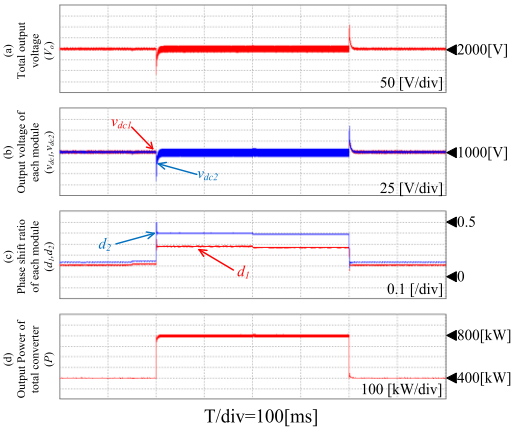

FIGURE 8. HSMC performance under different inductance conditions, (a) Overall DC output voltage. (b) Output voltages of two modules. (c) Phase-shift ratios. (d) Output power of IPOS modular converter.

Fig. 8 shows the performance of the HSMC in the case of different inductances, where the load is changed in steps from 400 kW to 800 kW and back to 400 kW. The overall DC output voltage is shown in Fig. 8(a), which well follows its reference. The overshoot and undershoot in transient states are less than 6%. Fig. 8(b) shows the output voltages of the two DAB modules, which are well controlled as 1000 V. Fig. 8(c) shows the phase-shift ratios of the two DAB modules, where d_1 and d_2 are different for the balancing control. Fig. 8(d) shows the output power of the IPOS modular DAB converter.

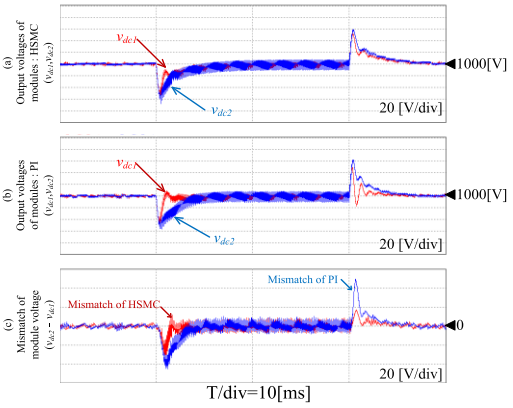

FIGURE 9. Responses of module voltages for the HSMC and PI control under unequal inductance. (a) Proposed controller. (b) PI controller. (c) Output voltage mismatch of DAB modules.

Fig. 9 illustrates the performance comparison of the HSMC and the PI control in transient conditions, where the load is changed from 400 kW to 800 kW and back to 400 kW under different inductance condition of the two DAB modules. Fig. 9(a) and (b) show the transient responses of output voltages of two DAB modules with the HSMC and PI control,

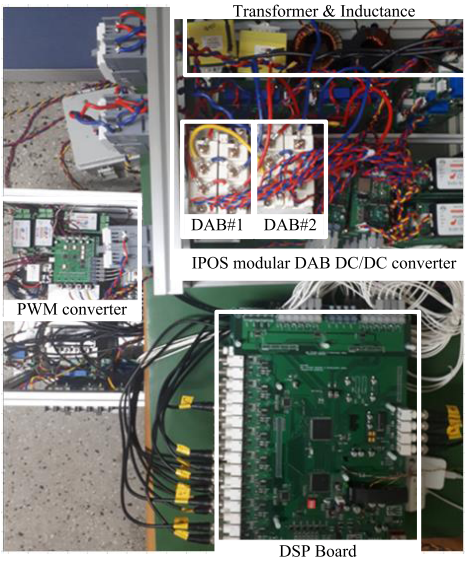

FIGURE 10. Experimental setup.

TABLE 3. Parameters of IPOS modular DAB converter (experiment).

Parameters	Values
Rated power	1250 W
LVDC bus voltage	100 V
MVDC bus voltage	200V
Number of modules	2

respectively. Fig. 9(c) shows the output voltage mismatch of two DAB modules. In the PI control, when the load is increased and decreased, the maximum voltage mismatches are about 45 V and 50 V, respectively. But, those of in the HSMC are only about 35 V and 17 V, respectively. As can be noted, the HSMC shows less sensitivity to the parameter mismatch than the PI control.

V. EXPERIMENTAL RESULTS

To prove the effectiveness of the proposed control algorithm, a down-scaled hardware set-up has been built at laboratory, as shown in Fig. 10. The parameters of the experimental hardware are listed in Table 3 and 4. To investigate the robustness of the proposed method, the equivalent series inductances of two DAB modules are set differently as $L_{s1} = 400\mu$H and $L_{s2} = 480\mu$H, respectively.

The HSM controller gains have been determined as $c_1 = c_3 = 6.12 \times 10^{-6}$, $c_2 = c_4 = 3.06 \times 10^{-3}$, n =1, and m=1620. For performance comparison, the PI controllers are employed, of which gains where the PI gains are determined based on a small signal analysis [31], which are listed in Table 5.

Fig. 11 shows the control performance in the case of with and without balancing controls under different inductance conditions, corresponding to Fig. 7. Fig. 11(a) and (b) show

TABLE 4. Parameters of single DAB module (experiment).

Parameters	Values
Rated power	625 W
Input DC voltage (v_i)	100 V
Output DC voltage (v_{dc1}, v_{dc2})	100 V
Transformer turn ratio	1 : 1
Equivalent series inductance of transformer referred to secondary side (L_{s1}, L_{s2})	400μH, 480μH
Output capacitance	50 μF
Switching frequency	5 kHz

TABLE 5. Parameters of single DAB module (experiment).

PI controllers (bandwidth)	Gains of bus voltage controller	Gains of balancing controller
PI-1 ($\omega_{c1} = 200Hz$)	$k_p = 0.0028$ $k_i = 1.738$	$k_p = 0.0056$ $k_i = 6.946$
PI-2 ($\omega_{c2} = 250Hz$)	$k_p = 0.0035$ $k_i = 2.1725$	$k_p = 0.007$ $k_i = 8.6825$
PI-3 ($\omega_{c3} = 300Hz$)	$k_p = 0.0042$ $k_i = 2.607$	$k_p = 0.0084$ $k_i = 10.419$

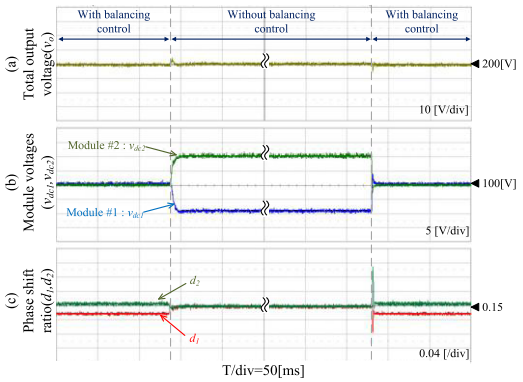

FIGURE 11. Control performance of with and without balancing controls under different inductance conditions. (a) DC-bus voltage. (b) Output voltages of two modules. (c) Phase-shift ratios of two modules.

the DC-bus voltage and the two module voltages, respectively. The DC-bus voltage is well controlled at 200 V regardless of the balancing control of each DAB module. Fig. 11(c) shows the phase-shift ratios of the two DAB modules.

Fig. 12 shows the control performance of the HSMC in the case of different inductances, where the load is changed from 285 W to 685 W and back to 285 W, which corresponds to

Fig. 8. Fig. 12(a) shows the DC-bust voltage, which follows its reference well. Fig. 12(b) shows the output voltages of the two DAB modules, which are closely controlled at 100 V. Fig. 12(c) shows the phase- shift ratios of the two DAB modules and Fig. 12(d) shows the output power of the IPOS modular DAB converter.

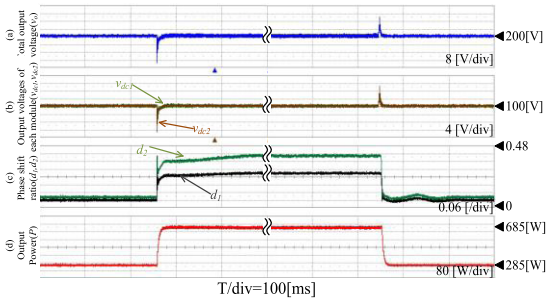

FIGURE 12. HSMC performance under different inductance conditions. (a) DC-bus voltage. (b) Output voltages of two modules. (c) Phase-shift ratios. (d) Output power of IPOS DAB converter.

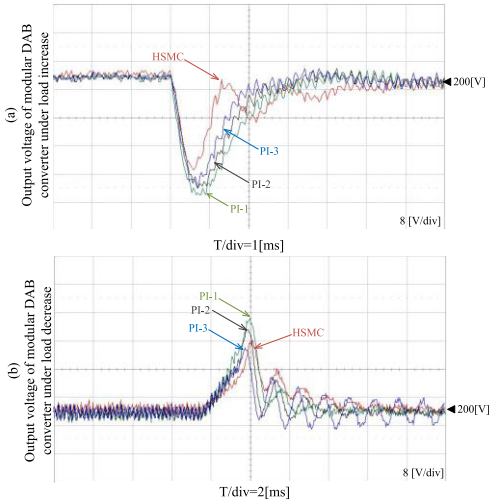

FIGURE 13. Comparison of DC-bus voltage control performance of the HSMC and PI control under different inductance conditions. (a) Load increase from 285 W to 685 W. (b) Load decrease from 685 W to 285 W.

Fig. 13 shows the DC-bus voltage responses of the HSMC and PI control when the load is changed from 285 W to 685 W and back to 285 W under unequal inductance condition. As can be seen, the HSMC gives faster transient responses and lower overshoot and undershoot than the PI control.

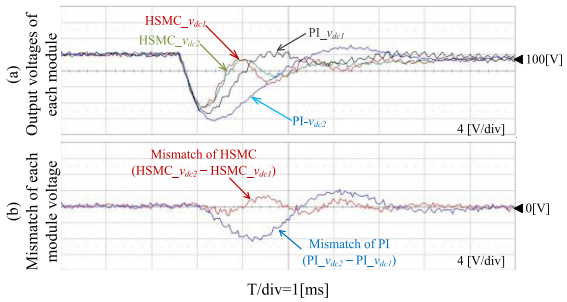

FIGURE 14. Control performance of module voltages for the HSMC and PI controller under different inductance conditions for load increases. (a) Module output voltages. (b) Mismatched module voltages.

Fig. 14 shows the voltage control performance of the HSMC and PI controller, where the transient condition is the same as that of in Fig. 13(a). Fig. 14(a) and (b) show the transient responses of two module voltages and the mismatched module voltages, respectively. In the PI control, the maximum

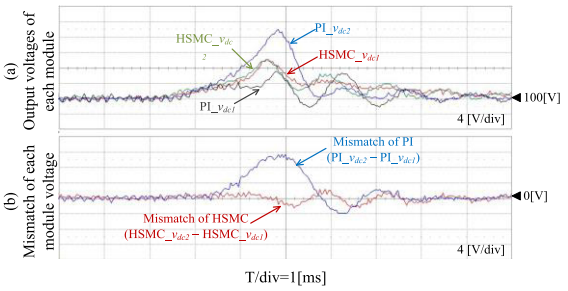

FIGURE 15. Control performance of module voltages for the HSMC and PI controller under different inductance conditions for load decreases. (a) Module output voltages. (b) Mismatched module voltages.

voltage mismatch is about 8 V. However, for the proposed HSMC, it is only about 2 V.

Fig. 15 shows the same quantities as in Fig. 14 when the load is decreased to 685 W from 285 W. In the PI control, the maximum voltage mismatch is 12 V, but that of in the HSMC is just 3 V. From Fig. 14 and 15, it is noticed that the HSMC gives more robust performance to parameter mismatch than the PI control.

VI. CONCLUSIONS

In this paper, a novel voltage control and balancing strategy of the IPOS modular DAB DC/DC converter has been proposed. At first, the mathematical model equation of the IPOS modular DAB converter has been developed in a state-space form. Next, the voltage controller has been designed by applying the HSMC theory to regulate the DC-bus voltage under the condition of mismatched inductances and to balance individual module voltages. The proposed scheme provides a balancing control capability of output voltages of individual modules as well as the DC-bus voltage control even with a parameter mismatch. Finally, the control performance of the proposed HSMC controller has been verified by simulation and experimental results. It is thought that the effectiveness of the developed hierarchical sliding mode controller is more remarkable for the IPOS modular DAB converter system with a large number of modules.

REFERENCES

[1] H. Fan and H. Li, "High-frequency transformer isolated bidirectional DC–DC converter modules with high efficiency over wide load range for 20 kVA solid-state transformer," *IEEE Trans. Power Electron.*, vol. 26, no. 12, pp. 3599–3608, Dec. 2011.

[2] F. M. Bahmani, T. Thiringer, A. Rabiei, and T. Abdulahovic, "Comparative study of a multi-MW high-power density DC transformer with an optimized high-frequency magnetics in all-DC offshore wind farm," *IEEE Trans. Power Del.*, vol. 31, no. 2, pp. 857–866, Apr. 2016.

[3] K. Sano and M. Takasaki, "A boost conversion system consisting of multiple DC-DC converter modules for interfacing wind farms and HVDC transmission," in *Proc. IEEE ECCE*, Sep. 2013, pp. 2613–2618.

[4] T. Cheng and D. D. C. Lu, "Three-port converters with a flexible power flow for integrating PV and energy storage into a DC bus," *J. Power Electron.*, vol. 17, no. 6, pp. 1433–1444, Nov. 2017.

[5] F. Krismer and J. W. Kolar, "Efficiency-optimized high-current dual active bridge converter for automotive applications," *IEEE Trans. Ind. Electron.*, vol. 59, no. 7, pp. 2745–2760, Jul. 2012.

[6] Z. Qin, Y. Shen, P. C. Loh, H. Wang, and F. Blaabjerg, "A dual active bridge converter with an extended high-efficiency range by DC blocking capacitor voltage control," *IEEE Trans. Power Electron.*, vol. 33, no. 7, pp. 5949–5966, Jul. 2018.

[7] B. J. Byen, B. H. Jeong, and G. H. Choe, "Single pulse-width-modulation strategy for dual-active bridge converters," *J. Power Electron.*, vol. 18, no. 1, pp. 137–146, Jan. 2018.

[8] L. Eitzen, C. Graf, and J. Maas, "Modular converter system for driving DEAP transducers," in *Proc. 15th Int. Power Electron. Motion Control Conf.*, Sep. 2012, p. LS7d.3-1-LS7d.3-8.

[9] Z. Haihua, D. Tran, S. S. Tuck, and A. M. Khambadkone, "Interleaved bi-directional dual active bridge DC-DC converter for interfacing ultracapacitor in micro-grid application," in *Proc. IEEE Int. Symp. Ind. Electron.*, Jul. 2010, pp. 2229–2234.

[10] T. Todorčević, P. Bauer, J. A. Ferreira, and R. van Kessel, "A modulation strategy for wide voltage output in DAB based DC-DC modular multilevel converter," in *Proc. 40th Annu. Conf. IEEE Ind. Electron. Soc.*, Oct. 2014, pp. 4514–4520.

[11] Y. Tang and A. Khaligh, "Bidirectional hybrid battery/ultracapacitor energy storage systems for next generation MVDC shipboard power systems," in *Proc. IEEE VPPC*, Sep. 2011, pp. 1–6.

[12] Y.-C. Jeung and D.-C. Lee, "Voltage and current regulation of bi-directional isolated dual active bridge DC-DC converters based on double-integral sliding mode control," *IEEE Trans. Power Electron* to be published, doi: 10.1109/TPEL.2018.2873834.

[13] G. Xu, D. S. Shang, and X. Z. Liao, "Decentralized inverse-droop control for input-series–output-parallel DC–DC converters," *IEEE Trans. Power Electron.*, vol. 30, no. 9, pp. 4621–4625, Sep. 2015.

[14] X. Yu, X. She, A. Huang, and L. Liu, "Distributed power balance strategy for DC/DC converters in solid state transformer," in *Proc. IEEE APEC*, Mar. 2014, pp. 989–994.

[15] L. Qu, D. L. Zhang, and Z. Y. Bao, "Active output-voltage-sharing control scheme for input series output series connected DC-DC converters based on a master slave structure," *IEEE Trans. Power Electron.*, vol. 32, no. 8, pp. 6638–6651, Oct. 2016.

[16] Z. Guo, D. Sha, and X. Liao, "Input voltage sharing control for input-series-output-parallel DC-DC converters without input voltage sensors," *J. Power Electron.*, vol. 12, no. 1, pp. 83–87, Jan. 2012.

[17] D. Sha, Z. Guo, and X. Liao, "Cross-feedback output-current-sharing control for input-series-output-parallel modular DC–DC converters," *IEEE Trans. Power Electron.*, vol. 25, no. 11, pp. 2762–2771, Nov. 2010.

[18] W. Yang, Z. Zhang, and S. Yang, "A new control strategy for input voltage sharing in input series output independent modular DC-DC converters," *J. Power Electron.*, vol. 17, no. 3, pp. 632–640, May 2017.

[19] Q. Wei, B. Wu, D. Xu, and N. R. Zargari, "Model predictive control of capacitor voltage balancing for cascaded modular DC–DC converters," *IEEE Trans. Power Electron.*, vol. 32, no. 1, pp. 752–761, Jan. 2017.

[20] Y. Xie, R. Ghaemi, J. Sun, and J. S. Freudenberg, "Model predictive control for a full bridge DC/DC converter," *IEEE Trans. Control Syst. Technol.*, vol. 20, no. 1, pp. 164–172, Jan. 2012.

[21] H. Zhou and A. M. Khambadkone, "Hybrid modulation for dual-active-bridge bidirectional converter with extended power range for ultracapacitor application," *IEEE Trans. Ind. Appl.*, vol. 45, no. 4, pp. 1434–1442, Jul./Aug. 2009.

[22] S. Talbi, A. M. Mabwe, and A. El Hajjaji, "PI-fuzzy control of a bidirectional dual active bridge converter," in *Proc. IEEE ACC*, May 2017, pp. 1271–1277.

[23] N. D. Dinh, N. M. Linh, N. D. Tuyen, and G. Fujita, "Observer-based nonlinear control for frequency modulated dual-active-bridge converter," in *Proc. IEEE ECCE*, Sep. 2016, pp. 1–8.

[24] M. J. Carrizosa, A. Benchaib, P. Alou, and G. Damm, "DC transformer for DC/DC connection in HVDC network," in *Proc. 15th Eur. Conf. Power Electron*, Sep. 2013, pp. 1–10.

[25] S. Talbi, A. M. Mabwe, and A. El Hajjaji, "Control of a bidirectional dual active bridge converter for charge and discharge of a Li-Ion Battery," in *Proc. IEEE 41st Ann. IEEE-IECON*, Nov. 2015, pp. 849–856.

[26] D. Sha, Z. Guo, T. Luo, and X. Liao, "A general control strategy for input-series–output-series modular DC–DC converters," *IEEE Trans. Power Electron.*, vol. 29, no. 7, pp. 3766–3775, Jul. 2014.

[27] W. Chen, X. Ruan, H. Yan, and C. K. Tse, "DC/DC conversion systems consisting of multiple converter modules: Stability, control, and experimental verifications," *IEEE Trans. Power Electron.*, vol. 24, no. 6, pp. 1463–1474, Jun. 2009.

[28] S. Lee, Y.-C. Jeung, and D.-C. Lee, "Output voltage regulation of IPOS modular dual active bridge DC/DC converters using sliding mode control," in *Proc. IEEE APEC*, Mar. 2018, pp. 3062–3067.

[29] R. W. A. A. De Doncker, D. M. Divan, and M. H. Kheraluwala, "A three-phase soft-switched high-power-density DC/DC converter for high-power applications," *IEEE Trans. Ind. Appl.*, vol. 27, no. 1, pp. 63–73, Jan./Feb. 1991.

[30] C. Mi, H. Bai, C. Wang, and S. Gargies, "Operation, design and control of dual H-bridge-based isolated bidirectional DC-DC converter," *IET Power Electron.*, vol. 1, no. 4, pp. 507–517, Dec. 2008.

[31] D. Segaran, B. P. McGrath, and D. G. Holmes, "Adaptive dynamic control of a bi-directional DC-DC converter," in *Proc. IEEE ECCE*, Sep. 2010, pp. 1442–1449.

[32] J.-J. Slotine and W. Li, *Applied Nonlinear Control*. Upper Saddle River, NJ, USA: Prentice-Hall, 1991.

[33] Y. Hao, J. Yi, D. Zhao, and D. Qian, "Robust control using incremental sliding mode for underactuated systems with mismatched uncertainties," in *Proc. Amer. Control Conf.*, Jun. 2008, pp. 532–537.

[34] S.-C. Tan, Y.-M. Lai, and C.-K. Tse, *Sliding Mode Control of Switching Power Converters: Techniques and Implementation*. Boca Raton, FL, USA: CRC Press, 2012.

[35] W. Wang, J. Yi, D. Zhao, and D. Liu, "Design of a stable sliding-mode controller for a class of second-order underactuated systems," *IEE Proc.-Control Theory Appl.*, vol. 151, no. 6, pp. 683–690, Nov. 2004.

[36] B. Liu, M. Yue, and R. Liu, "Motion control of an underactuated spherical robot: A hierarchical sliding-mode approach with disturbance estimation," in *Proc. ICMA*, Aug. 2012, pp. 1804–1809.

SANGMIN LEE received the B.S. and M.S. degrees in electrical engineering from Yeungnam University, Gyeongsan, South Korea, in 2015 and 2017, respectively. He is currently with Doosan Robotics Co., Ltd., Suwon, South Korea. His current research interests include modular dc–dc converters and machine control.

YOON-CHEUL JEUNG (S'14) received the B.S. and M.S. degrees in electrical engineering from Yeungnam University, South Korea, in 2010 and 2013, respectively, where he is currently pursuing the Ph.D. degree with the Power Electronics and Machine Control Laboratory. His current research interests include the control of power converters and power quality.

DONG-CHOON LEE (S'90–M'95–SM'13) received the B.S., M.S., and Ph.D. degrees in electrical engineering from Seoul National University, Seoul, South Korea, in 1985, 1987, and 1993, respectively. He was a Research Engineer with Daewoo Heavy Industry, South Korea, from 1987 to 1988. He was a Visiting Scholar with the Power Quality Laboratory, Texas A&M University, College Station, TX, USA, in 1998; with the Electrical Drive Center, University of Nottingham, Nottingham, U.K., in 2001; with the Wisconsin Electric Machines and Power Electronics Consortium, University of Wisconsin, Madison, WI, USA, in 2004; and also with the FREEDM Systems Center, North Carolina State University, Raleigh, NC, USA, from 2011 to 2012. He has been a Faculty Member with the Department of Electrical Engineering, Yeungnam University, Gyeongsan, South Korea, since 1994. His current research interests include power converter design and control, renewable energy and grid connection, ac machine drives, and power quality. From 2015 to 2017, he served as the Editor-in-Chief for the *Journal of Power Electronics* of the Korean Institute of Power Electronics, where he is currently the President.